An Investigation of Quality Aspects of Noisy Colour Images for Iris Recognition

G. McConnon, F. Deravi, S. Hoque, K. Sirlantzis, G. Howells

School of Engineering and Digital Arts, University of Kent,Canterbury, UK
{gm242, f.deravi, s.hoque, k.sirlantzis, w.g.j.howells} @kent.ac.uk

Abstract

The UBIRIS.v2 dataset is a set of noisy colour iris images designed to simulate visible wavelength iris acquisition at-a-distance and on-the-move. This paper presents an examination of some of the characteristics that can impact the performance of iris recognition in the UBIRIS.v2 dataset. This dataset consists of iris images in the visible wavelength and was designed to be noisy. The quality and characteristics of these images are surveyed by examining seven different channels of information extracted from them: red, green, blue, intensity, value, lightness, and luminance. We present new quality metrics to assess the image characteristics with regard to focus, entropy, reflections, pupil constriction and pupillary boundary contrast. The results clearly suggest the existence of different characteristics for these channels and could be exploited for use in the design and evaluation of iris recognition systems.

Keywords: *UBIRIS.v2 dataset, iris recognition, iris recognition systems.*

1. Introduction

The majority of iris recognition (IR) systems have used near-infrared illumination (NIR, 700-900nm) [1] to sense the stroma of the iris rather than visible wavelength light. NIR has the advantage of not stimulating the melanin found within the stroma and thus reveals a clearer image of its structure. It also has other advantages including the following: It is undetectable to the human eye [2], has low scleral reflectance [1] and fewer corneal reflections [3] and is much less susceptible to ambient reflections in general. An example of this is shown in Figure 1.

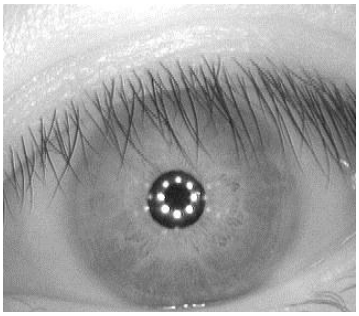

Figure 1. A Near-infrared iris image, CASIA [4] dataset

It also has some significant disadvantages, the most pertinent of which being the need for specialized cameras with NIR illumination. If IR is to become seamlessly ubiquitous and integrated into the daily lives of the general public, it must take advantage of technologies already in place. In particular, mobile phones containing cameras with up to 12 megapixel sensors [6] are currently available. The potential for these devices to be used as mobile personal IR systems is staggering and so the implications of using visible wavelength images for IR and their potential impact on image quality needs to be examined.

To the casual observer the most striking differences between NIR and visible wavelength images is the iris colour. This is commonly represented as a blend of red, green and blue channels in the RGB colour space for example [5]. Other representations such as CMYK (Cyan, Magenta, Yellow, and Key) also exist. In this paper however, we have chosen to examine RGB. In this colour space each channel is a grayscale image representing the intensity values of that band of wavelengths, e.g., red is the band from approximately 630 to 700 nm, green from 490 to 560 nm, and blue from 450 to 590 nm [6]. Figure 2, (a) through (c) show examples of these from the same image taken from the UBIRIS.v2 [7] dataset. Colour images are often converted to black and white images with a single value representing the overall intensity of each pixel. These grayscale channels can be calculated in a number of different ways and so we decided to include in our study a selection of these as can be seen in Figure 2, (d) through (g).

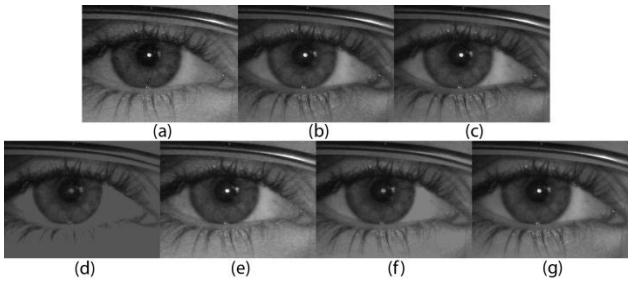

Figure 2. Grayscale representations of an image from the UBIRIS.v2 [7] dataset in different channels: (a) Red, (b) Green, (c) Blue, (d) Intensity, (e) Value, (f) Lightness, and (g) Luminance.

Iris colour is determined by the amount, and type, of melanin synthesised in the stroma [8]. Irides with low levels of melanin appear blue because the stroma itself reflects short wavelength blue light. The dominant form of melanin in the human iris is Eumelanin which has a brown to black hue. Pheomelanin, which is less common, has a yellow to red hue. Irides with no pigmentation appear red due to the colour of the underlying blood vessels. Brown is the dominant eye colour in humans worldwide [9]. However, in Iceland over 80% of the population have either blue or green irides [9,10].

Eumelanin is most fluorescent under visible wavelength light and this means more noise is included from specular reflections and shadows but it also allows a more detailed representation to be acquired [1]. In addition to this, under mobile, iris-on-the-move, conditions where the user is not expected to be an expert and the acquisition device may be a smart phone or other hand-held device, other forms of noise and distortion such as motion blur, occlusion by eyelids and eyelashes, and defocus will have impact. In these conditions, quality assessment of the acquired image will have a significant role to play in both optimizing the system to take best advantage of the acquired image and in providing feedback to the user on the acquisition process. UBIRIS.v2 [7] was designed, with this kind of scenario

in mind, to be a noisy dataset. An example of a particularly poor quality images can be seen in Figure 3.

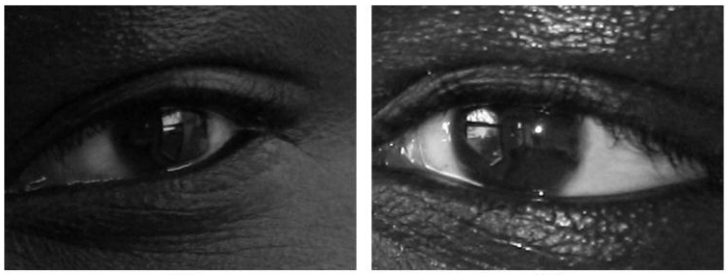

Figure 3. Poor quality visible wavelength imagse from the UBIRIS.v2 [7] dataset. Both have diffuse-source reflections obscuring part of the iris. There is almost no difference in contrast between the pupil and iris at the pupillary boundary of (a) and (b) shows high intensity regions on the skin which could misleadingly be detected as PSRs.

In this article we continue the work of surveying the quality traits of the UBIRIS.v2 dataset, which we began with a previous publication on point-source reflections [11]. In Section 2 we will discuss the channels of information extracted from the captured images and the quality metrics proposed and examined in this paper in more detail. This is followed by a description of the implementation of the study in Section 3. The results are represented in Section 4 and finally some conclusions and suggestions for further work are discussed in Section 5

2. Channels and Quality Metrics

What follows is a description of the methods used to extract the various channels from the images and the metrics used to evaluate the quality of those images. Where possible we applied these metrics globally, to the entire image, and locally, to the iris/pupil region only. With the exception of entropy, all metrics are in the range $[0,1]$ with 0 being worst and 1 being best case.

2.1. Intensity channels

In addition to the red, *R*, green, *G*, and blue, *B*, channels extracted from the captured images, we examined four ways of encoding grayscale intensity channels: intensity (1)[5], value (2)[12], lightness (3)[13], and luminance (4)[14].

$$I = (R + G + B)/3 \quad (1)$$

$$V = max(R, G, B) \quad (2)$$

$$L = \big(max(R, G, B) + min(R, G, B)\big)/2 \quad (3)$$

$$Y = 0.2126\,R \;+\; 0.7152\,G \;+\; 0.0722\,B \quad (4)$$

2.2. Focus

We used the method described by Daugman [15] to assess focus. It takes advantage of the fact that defocused images tend to have lower frequency content. Daugman describes an

8×8 convolution kernel, shown in Figure 4, which acts as a band pass filter and can be used to assess focus.

Essentially this kernel is convolved with the image which is then squared and accumulated in x before it is passed through (5), where c is the x value of the image chosen to exemplify half focus, to produce a normalized focus score $f(x)$ in the range [0,100]. For our purposes we prefer to keep the focus score (FS) in the range [0,1] and so use (6) instead.

$$f(x) = 100(x^2/(x^2 + c^2)) \quad (5)$$

$$FS = (x^2/(x^2 + c^2)) \quad (6)$$

1	1	1	1	1	1	1	1
1	1	1	1	1	1	1	1
1	1	3	3	3	3	1	1
1	1	3	3	3	3	1	1
1	1	3	3	3	3	1	1
1	1	3	3	3	3	1	1
1	1	1	1	1	1	1	1
1	1	1	1	1	1	1	1

Figure 4. Daugman's 8×8 focus assessment kernel

Kang and Park [16,17] and Wei *et al.* [18] proposed using other kernels for increased speed and sensitivity, however, we look here only at the kernel proposed by Daugman.

2.3. Point-source reflections

Specular reflections come in two forms: diffuse-source reflections, caused by scattered ambient light, and point-source reflections (PSRs), usually caused by highly localized sources such as desk lamps or overhead lighting [11]. With diffuse-source reflections the underlying image remains partially visible and the affected area can be quite large. PSRs are usually smaller high-intensity regions with semi-transparent borders. Figure 5 includes examples of both forms of specular reflection.

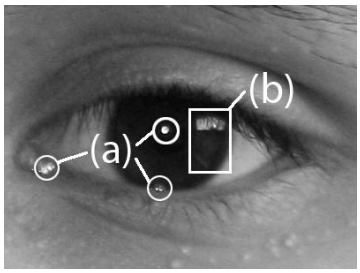

Figure 5. This image from UBIRIS. v2 [7] shows three point-source reflections (a) and a diffuse-source reflection (b).

Most detection methods use intensity thresholding to take advantage of the PSR's high intensity characteristic. Tan et al. [19] considered the brightest 5% of pixels in the image to be

PSRs. For Almeida [20] any pixel with an intensity value above 250 was designated as a PSR. Sankowski et al. [21] based their threshold T_{ref} on equation (7).

$$T_{ref} = I_{ave} + P \cdot (I_{max} - I_{ave}) \tag{7}$$

where $P \in (0,1)$, I_{ave} is the average intensity of the image pixels and I_{max} is the average of the brightest 4% of image pixels. They then used dilation, to incorporate the semi-transparent border, and connect neighbouring regions using closure.

We can create a normalized metric from these using (8).

$$Q_{psr} = {A_{psr}}/{A_{iris}} \tag{8}$$

where Q_{psr} is our PSR measure, $A_{psr}$is the total area in pixels of the PSRs and $A_{iris}$is the area in pixels of the iris including the pupil.

Global estimation of PSRs was found to be misleading as can be seen from Figure 3b.

2.4. Entropy

Shannon and Weaver [22] introduced (9), the equation of 1st order entropy of a signal, as a measure of uncertainty in a signal. It can be thought of as how much information is conveyed by a signal.

$$H(X) = -\sum_{i=1}^{n} p(x_i) log\ p(x_i) \tag{9}$$

where X is a grayscale image, $p(x_i)$ is the probability that a pixel in X will have the value x_i.

We looked at both the global (where X was the entire image) and local (where X covered the iris region only) entropy of the image.

2.5. Iris and Pupil Dimensions

Iris and pupil dimensions can impact segmentation and IR performance. Proenca and Alexander [23] found that reducing iris area to 30% of the size of the unwrapped image significantly impacts error rates. Daugman [15] found that irides of 70 pixels radius minimum should be used for IR in NIR.

We therefore propose (10) as a measure for iris diameter quality.

$$I_{\emptyset} = \frac{\mathrm{D_i}}{\mathrm{D_i} + \mathrm{d}} \tag{10}$$

where $\mathrm{D_i}$ is the diameter of the iris and $\mathrm{d} = 140$ or effectively double the minimum radius suggested by Daugman. $I_{\emptyset}$ has the range [0,1) with anything greater than 0.5 having more than the minimum suggested diameter.

Wyatt [24] states that the human iris has an approximate diameter of 12 mm and that pupil diameter can vary from 1.5 – 7.5 mm or 12 – 60% of iris diameter. This is usually

compensated for using Daugman's rubber sheet model [25] in which the Cartesian coordinates of the iris are converted to a form of dimensionless polar coordinate system.

However Ma *et al.* [26] found that 10.7% of false non-matches in their experiments involved images with excessive pupil dilation. For Hollingsworth *et al.* [27-29] performance was degraded when there was a disparity between pupil dilations but also between images of similar dilation as the dilation increased. Thornton *et al.* [30] used (11) to measure pupil dilation and show that dilation is not perfectly linear along the radial direction and so dilation can cause pattern deformation.

$$M_1 = 100 \times \frac{R_p}{R_i} \tag{11}$$

where R_p is the pupil radius and R_i is the iris radius.

Lili and Mei [31] use a similar method to assess pupil dilation (12) or more precisely pupil constriction C. The smaller C is the more dilated the iris.

$$C = 1 - \frac{R_p}{R_i} \tag{12}$$

where R_p is the pupil radius and R_i is the iris radius. This is the measure we used for our quality assessment.

2.6. Pupillary Boundary Contrast

In unconstrained systems illumination may vary wildly and in visible wavelength systems subjects with dark irides have very low contrast at the pupil boundary [32]. This is well illustrated in Figure 3 and **Error! Reference source not found.**. Mottalli *et al.* [33] measured contrast across the pupillary boundary and used this as an indication of image focus.

We propose using pupillary boundary contrast as a measure of how easily the pupil can be segmented from the rest of the image. Given the boundary in polar form (13) we use the metric P_d given in (14) and illustrated in Figure 6.

$$P(\theta, \rho) = I\left(x_p + \rho \cdot cos\theta, y_p + \rho \cdot sin\theta\right) \tag{13}$$

$$P_d = \left(\frac{1}{n}\sum_{\theta}(P_2 - P_1)\right) \Big/ 256 \tag{14}$$

where I is the grayscale image, $\left(x_p, y_p\right)$ are the centre coordinates of the pupil, ρ is the radius of the pupil, n is the number of samples of θ, $P_1 = P(\theta, \rho - \varepsilon)$ and $P_2 = P(\theta, \rho + \varepsilon)$.

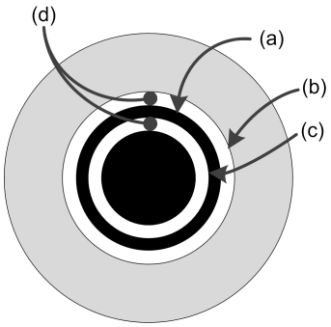

Figure 6. In this image (a) is the pupillary boundary, (b) and (c) are circles ± 1 pixel radius from (a). Pupil Boundary Contrast is the average difference between opposing pairs (d) of pixels in (b) and (c) divided by the maximum value possible.

3. Implementation

Initial attempts to segment the dataset were made using the method developed by Masek and Kovesi [34]. However, this failed to segment the majority of the images correctly. In particular, it had trouble identifying the pupil in images where the pupillary boundary contrast was low.

For this reason we decided to create a ground truth by segmenting the images manually. In images where the boundary of the iris or pupil could not be discerned completely the boundary in question was assumed to be circular and segmented based on whatever boundary information was available. In some extreme cases neither the pupil nor irises were distinguishable. These were designated as Out-of-Iris images.

In total 11,104 images were segmented and the ground truth data we produced is available on request for academic use.

4. Results

4.1. Global Focus Scores

We first looked at global focus scores *FS* in each of the seven channels. The results are shown in Figure 7 as histograms of the focus scores for each channel. It can be seen that for the red, blue, green, value and luminance channels the *FS* trends were quite similar.

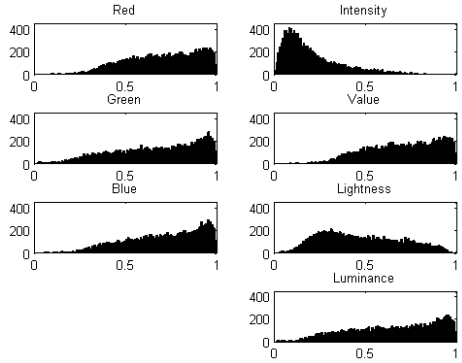

Figure 7. Global Focus Histograms (X-axis: global focus score; Y-axis: number of images)

However, lightness and particularly intensity channels seem to have degraded FS scores. This is most likely caused by the averaging effect of conversion to these channels. This can be seen clearly in Figure 8.

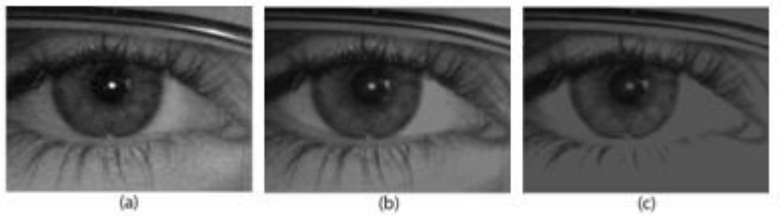

Figure 8. The channels shown here are Red (a), Value (b) and Intensity (c). The averaging effect of conversion from RGB to value or intensity can be seen clearly.

4.2. Local point-source Reflection

As previously stated, we found global PSR measurements to be deceptive due to significant amounts of reflection from the sclera and skin as shown in **Error! Reference source not found.**. So we concentrate here on local PSR scores. As can be seen from Figure 9, the red, green and blue channels have similar scores. Value seems to fare best with almost all of its images scoring $Q_{psr} = \sim 0.95$. Lightness and luminance also have most images with $Q_{psr} = \sim 0.95$, while the intensity channel seems to suffer the most with scores going below $Q_{psr} = 0.6$.

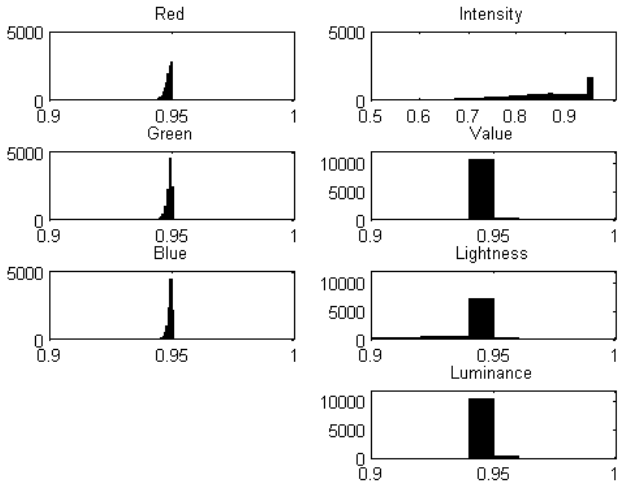

Figure 9. Local Point-source Reflection Histograms (X-axis: local PSR score; Y-axis: number of images)

4.3. Entropy

With global entropy, Figure 10, again the red, blue, green, value and luminance channels all seem to behave similarly with red, value and luminance having slightly higher entropy scores. Intensity and lightness both have more spread out scores with almost all of intensity's scores lower than the main group of channels.

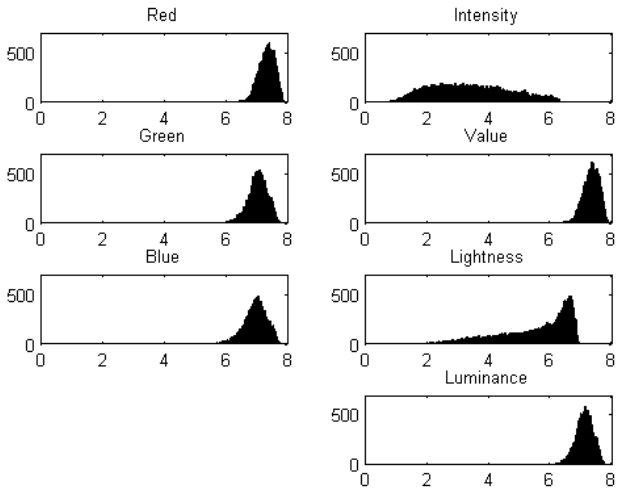

Figure 10. Global Entropy Histograms (X-axis: number of entropy bits; Y-axis: number of images)

Local entropy scores are slightly lower than their global counterparts. Intensity and lightness again buck the trend by having lower and less spread out scores, although still lower than the other channels.

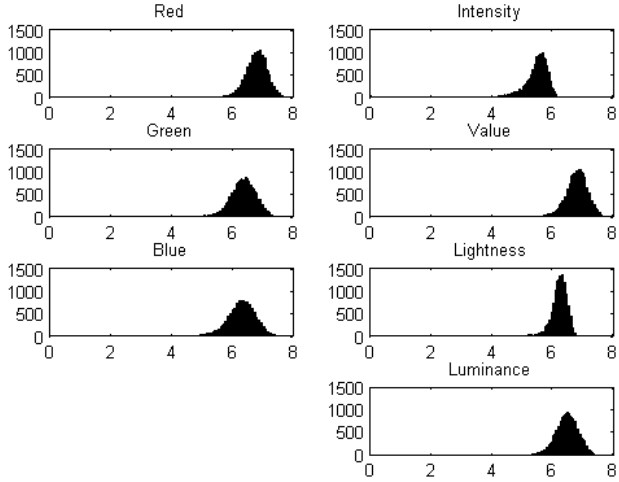

Figure 11. Local Entropy Histograms (X-axis: number of entropy bits; Y-axis: number of images)

4.4. Iris and Pupil Dimensions

We first looked at the distributions of pupil and iris diameters. Figure 12 shows the actual diameters in pixels while Figure 13 shows the normalized iris diameter, $I_{\emptyset}$, and the pupil constriction, C.

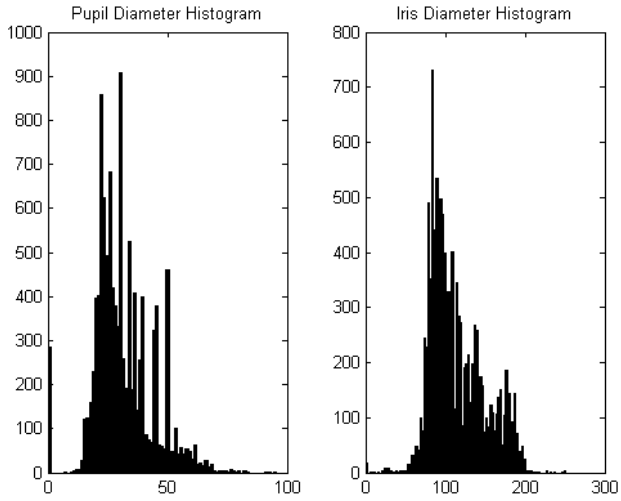

Figure 12. Pupil Diameter Histogram and Iris Diameter Histogram (X-axis: diameter in pixels; Y-axis: number of images)

The majority of pupils were less than 50 pixels in diameter and those indicated as zero in Figure 12 were from either Out-of-Iris images or images in which the pupillary boundary contrast was so low that it was impossible to segment.

The iris diameters were mostly below the suggested value $d = 140$ as can be seen from both Figure 12 and Figure 13. In both cases, images with scores of zero were Out-of-Iris images. Most images had constriction values above 0.6. Those images in which C=1 are either Out-of-Iris images or images in which the pupillary boundary contrast extremely low.

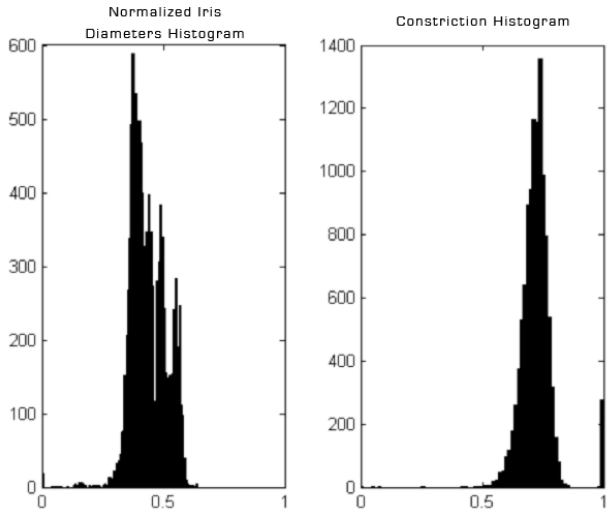

Figure 13. Normalized Iris Diameters and Constriction Ratio Histograms (X-axis: metric score; Y-axis: number of images)

Although the constriction scores are reasonable the diameter scores suggest that for the vast majority of images there may not be not enough iris content for accurate recognition.

4.5. Pupillary Boundary Contrast

As expected the pupillary boundary contrast scores were all consistently low with few images achieving scores higher than 0.1. The red and value channels seem to have done slightly better than the other channels with more images with $P_d > 0.05$. The blue channel had the worst scores with 71% of images scoring $P_d > 0.02$.

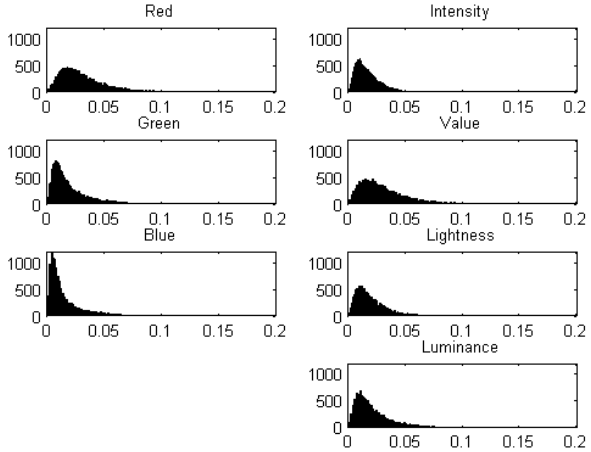

Figure 14. Pupillary Boundary Contrast Histograms (X-axis: pupillary boundary contrast score; Y-axis: number of images)

5. Conclusions

The UBIRIS.v2 dataset is challenging for IR for many reasons. In this paper we examined a selection of possible factors which may impact IR performance. We introduce new metrics for evaluating the iris area affected by point-source reflections, iris diameter and pupillary boundary contrast. We also examined focus, entropy and constriction using measures found in the literature. These metrics were evaluated using seven different channels (red, blue, green, intensity, value, lightness and luminance).

From our preliminary investigations no linear law was found between these metrics' scores and segmentation or recognition evaluation. However they suggest that further work on the fusion of these metrics to produce a scalar value for the assessment of image quality for IR and the impact of these covariates on the main methods used for the extraction of features for IR could lead to increased accuracy and usability of IR, particularly with on-the-move and at-a-distance systems.

Acknowledgement

This work is part of the NOmad Biometric Authentication (NOBA) project funded by ERDF under the Interreg IVA program. Reference No. 4051.

References

[1] H. Proença and L.A. Alexandre, "Introduction to the Special Issue on the Segmentation of Visible Wavelength Iris Images Captured At-a-distance and On-the-move," *Image and Vision Computing*, vol. 28, pp. 213-214, Feb. 2010.

[2] C. Boyce et al., "Multispectral iris analysis: a preliminary study," in *IEEE Conference on Computer Vision and Pattern Recognition*, 2006, pp. 51–51.

[3] M.S. Hosseini, B.N. Araabi, and H. Soltanian-Zadeh, "Pigment Melanin: Pattern for Iris Recognition," *0911.5462*, Nov. 2009.

[4] Inst. of Automation, Chinese Academy of Sciences. (2006). *Note on CASIA-IrisV3* [Online]. Available: http://www.cbsr.ia.ac.cn/english/IrisDatabase.asp [Accessed: 2009, November, 5].

[5] R.C. Gonzalez and R.E. Woods, *Digital Image Processing by Gonzalez*. Upper Saddle River, NJ: Prentice Hall, 2001.

[6] C.F. Bohren and E.E. Clothiaux, *Fundamentals of atmospheric radiation: an introduction with 400 problems*. Wiley-VCH, 2006.

[7] H. Proença et al., "The UBIRIS.v2: A Database of Visible Wavelength Images Captured On-The-Move and At-A-Distance," *IEEE Trans. Pattern Anal. Mach. Intell.*, vol. PP, p. 1, 2009.

[8] P.D. Imesch, I.H.L. Wallow, and D.M. Albert, "The color of the human eye: A review of morphologic correlates and of some conditions that affect iridial pigmentation," *Survey of Ophthalmology*, vol. 41, p. S117-S123, Feb. 1997.

[9] P. Sulem et al., "Genetic determinants of hair, eye and skin pigmentation in Europeans," *Nature Genetics*, vol. 39, pp. 1443-1452, Dec. 2007.

[10] V. Rafnsson et al., "Risk factors for malignant melanoma in an Icelandic population sample," *Preventive Medicine*, vol. 39, pp. 247-252, Aug. 2004.

[11] G. McConnon et al., "A Survey of Point-Source Specular Reflections in Noisy Iris Images," in *International Conference on Emerging Security Technologies*, 2010, pp. 13–17.

[12] A.R. Smith, "Color gamut transform pairs," *SIGGRAPH Comput. Graph.*, vol. 12, pp. 12–19, Aug. 1978.

[13] H. Levkowitz and G.T. Herman, "GLHS: A Generalized Lightness, Hue, and Saturation Color Model," *CVGIP: Graphical Models and Image Processing*, vol. 55, pp. 271-285, Jul. 1993.

[14] C. Poynton, "The rehabilitation of gamma," *Human Vision and Electronic Imaging III*, pp. 232–249, 1998.

[15] J. Daugman, "How iris recognition works," *IEEE Trans. Circuits Syst. Video Technol.*, vol. 14, pp. 21-30, 2004.

[16] B.J. Kang and K.R. Park, "A robust eyelash detection based on iris focus assessment," *Pattern Recognition Letters*, vol. 28, pp. 1630-1639, Oct. 2007.

[17] B.J. Kang and K.R. Park, "Real-Time Image Restoration for Iris Recognition Systems," *Systems, Man, and Cybernetics, Part B: Cybernetics, IEEE Transactions on*, vol. 37, pp. 1555-1566, 2007.

[18] Z. Wei et al., "Robust and fast assessment of iris image quality," *Proceedings Advances in Biometrics*, vol. 3832, pp. 464-471, 2006.

[19] T. Tan, Z. He, and Z. Sun, "Efficient and robust segmentation of noisy iris images for non-cooperative iris recognition," *Image and Vision Computing*, vol. 28, pp. 223-230, 2010.

[20] P. de Almeida, "A knowledge-based approach to the iris segmentation problem," *Image and Vision Computing*, vol. 28, pp. 238-245, Feb. 2010.

[21] W. Sankowski et al., "Reliable algorithm for iris segmentation in eye image," *Image and Vision Computing*, vol. 28, pp. 231-237, Feb. 2010.

[22] C.E. Shannon and W. Weaver, "The mathematical theory of communication University of Illinois Press," *Urbana*, vol. 111, 1949.

[23] H. Proença and L.A. Alexandre, "Iris Recognition: An Analysis of the Aliasing Problem in the Iris Normalization Stage," in *Computational Intelligence and Security, 2006 International Conference on*, vol. 2, 2006, pp. 1771-1774.

[24] H. Wyatt, "A 'minimum-wear-and-tear' meshwork for the iris," *Vision Research*, vol. 40, pp. 2167-2176, Jul. 2000.

[25] J.G. Daugman, "High confidence visual recognition of persons by a test of statistical independence," *IEEE Trans. Pattern Anal. Mach. Intell.*, vol. 15, pp. 1148-1161, 1993.

[26] L. Ma et al., "Efficient iris recognition by characterizing key local variations," *Image Processing, IEEE Transactions on*, vol. 13, pp. 739-750, 2004.

[27] K. Hollingsworth, K. Bowyer, and P. Flynn, "The Importance of Small Pupils: A Study of How Pupil Dilation Affects Iris Biometrics," *2008 IEEE Second International Conference On Biometrics: Theory,*, pp. 61-66, 2008.

[28] K. Hollingsworth, K.W. Bowyer, and P.J. Flynn, "Pupil dilation degrades iris biometric performance," *Computer Vision and Image Understanding*, vol. 113, pp. 150-157, Jan. 2009.

[29] K.W. Bowyer et al., "Factors that degrade the match distribution in iris biometrics," *Identity in the Information Society*, vol. 2, pp. 327-343, Dec. 2009.

[30] J. Thornton, M. Savvides, and V. Kumar, "A Bayesian Approach to Deformed Pattern Matching of Iris Images," *IEEE Trans. Pattern Anal. Mach. Intell.*, vol. 29, pp. 596-606, 2007.

[31] P. Lili and X. Mei, "The algorithm of iris image preprocessing," in *Fourth IEEE Workshop on Automatic Identification Advanced Technologies*, IEEE, 2005, pp. 134-138.

[32] M. Shamsi et al., "Fast Algorithm for Iris Localization Using Daugman Circular Integro Differential Operator," *2009 International Conference of Soft Computing and Pattern Recognition*, pp. 393-398, 2009.

[33] M. Mottalli, M. Mejail, and J. Jacobo-Berlles, "Flexible Image Segmentation And Quality Assessment For Real-Time Iris Recognition," *2009 16th IEEE International Conference on Image Processing, Vols 1-6*, pp. 1921-1924, 2009.

[34] Masek, Libor and P. Kovesi. *Libor Masek* [Online]. Available: http://www.csse.uwa.edu.au/~pk/studentprojects/libor/ [Accessed: 2010, October, 21].

Authors

George McConnon obtained his first degree in Computer Systems Engineering from the University of Kent, Canterbury in 2009. His final year project was to develop a system for interactive passport image acquisition for which he received the BAE Systems Prize for Most Outstanding Project. In 2008 he worked as a student placement with Oxford Semiconductor's Research and Development group. In 2009 he began wo rking on his Ph.D. on Image Quality for Iris Recognition at the University of Kent, Canterbury.

Dr. Farzin Deravi worked from 1983 to 1987 as a research assistant at the University of Wales, Swansea where he obtained his Ph.D. In 1987 he joined the academic staff at Swansea where at the Department of Electrical and Electronic Engineering. In 1998 he joined University of Kent whe re he is Reader in Information Engineering. He was the 13 founding chair of the IET Professional Network on Visual Information Engineering.

Dr. Sanaul Hoque obtained his first degree from Bangladesh University of Engineering & Technology (BUET) in Electrical & Electronic Engineering in 1991. He also obtained an MSc in Computer Engineering from the same institute. He was awarded a PhD in Electronic Engineering at University of Kent, UK where he is currently working as a faculty. Dr Hoque's research interests include im age processing & computer vision, OCR, biometrics, biometric encryption, multi-expert fusion.

Dr. Konstantinos Sirlantzis has worked for a number of years within the Image Processing and Vision Research Group at University of Kent, contributing significantly to the generic work on classifier combination and optimization. Dr Sirlantzis holds an MSc in Statistics and a PhD in Operational R esearch. He is a Fellow of the Royal Statistical Society, a Member of the Institution of Electrical Engineers (IEE) and of the IEE Visual Information Processing Professional Network.

Dr. Gareth Howells has been involved in research relating to image processing, artificial neural networks and pattern recognition for twenty years. He has developed several novel pattern classification systems employing both weightless and logic based artificial neural network technologies. In addition, previous work has focused on merging of techniques taken from formal mathematics and formal logic with existing algorithms pertaining to Artificial Evolutionary Systems..